RSC Publishing Faraday Discussions

Hydration Motifs of Ammonium Bisulfate Clusters of Relevance to Atmospheric New Particle Formation

Journal:	*Faraday Discussions*
Manuscript ID	FD-ART-11-2018-000206.R1
Article Type:	Paper
Date Submitted by the Author:	18-Jan-2019
Complete List of Authors:	Yang, Yi; Stony Brook University, Chemistry Johnson, Christopher; Stony Brook University, Chemistry

Hydration Motifs of Ammonium Bisulfate Clusters of Relevance to Atmospheric New Particle Formation

Yi Yang and Christopher J. Johnson

Department of Chemistry, Stony Brook University, Stony Brook, NY 11794-3400

Clusters of ammonia or amines and sulfuric acid are predicted to drive the formation of new particles from atmospheric trace gases, but the role of water in this process, or even the extent of hydration of the clusters, is not well known. We present vibrational spectra of exactly mass-selected clusters of ammonia or dimethylamine and sulfuric acid with zero to four water molecules bound. These hydrated clusters are synthesized by storing initially-dry clusters in an ion trap held at 180 K with a small partial pressure of water vapor. Analysis of the spectra shows that hydration occurs first at the ammonium NH groups, rather than the bisulfate OH or between the conjugate acids and bases, and that binding to the bisulfate OH only becomes favorable if an additional hydrogen bond acceptor is in the vicinity. These spectra are compared to quantum chemical predictions to evaluate the specific structural motifs present. Broadly speaking, they reveal classes of isomers with similar overall binding motifs but different specific arrangements of water within these motifs. The structures determined for each ensuing hydrate can be explained by addition of one water to the next lower hydrate, without the need for significant rearrangement of the cluster or hydrate structures. Taken together, these observations suggest that multiple hydration isomers may play a role in atmospheric conditions, but substantial barriers to water rearrangement may direct the mechanism of sequential hydration, and entropic contributions to the heats of formation may play an important role in models of new particle formation.

I. Introduction

Atmospheric new particle formation (NPF) is the process by which atmospheric trace gases cluster and grow into climatically-relevant particles.[1, 2] The effect of these new particles on the climate is unclear - while they contribute to the overall balance of aerosol in the atmosphere, which has been predicted to be a cooling influence,[3] recent simulations suggest that in their formation they scavenge vapors, thereby reducing cloud brightness and potentially behaving as a net warming impact.[4] Furthermore, the role of water is particularly unclear due to difficulties in directly measuring the hydration of new particles.[5, 6] Thus, a detailed understanding of the chemical mechanism underlying NPF is needed to fully determine their climatic effects.

Though it was initially expected to involve sulfuric acid and water,[7-11] more recent field observations and laboratory experiments have confirmed that NPF primarily is driven by acid-base chemistry between sulfuric acid,[12-15] ammonia and amines,[16-18] organic acids,[19, 20] and a growing list of other atmospheric vapors. Thermodynamic models of growth,[21, 22] using results from quantum chemical calculations,[23, 24] give formation rates of similar orders of magnitude to those found in atmospheric simulation chambers for several compositions.[23, 24] The computed structures of clusters of amines and sulfuric acid show that proton transfer is nearly complete, resulting in significant stabilization from Coulomb attraction that leads to reduced evaporation rates of particle constituents.[25-30] More recently, the more basic diamines have been proposed to further enhance particle formation by significantly stabilizing the particles, potentially growing at the collision limit.[24, 31, 32]

As the list of species potentially involved in NPF has grown,[18, 33-36] the role of water in NPF has become less apparent. While NPF rates depend on relative humidity, this dependence is not particularly strong.[37, 38] Direct detection of water on clusters in atmospheric simulation experiments is difficult, as any water that may be present likely evaporates during the sampling process.[39] Quantum chemical calculations predict that new particles are likely to feature up to several water molecules, but it is unclear whether the surface-bound water plays a substantial role in the mechanism of growth.[28-30, 40, 41] These calculations are complicated by the large structural configuration space that must be searched when screening for candidate geometries.[42-44] Analysis of the role of hydration in thermodynamic models of particle growth have yielded unclear results, with changes in growth rates due to water showing high variability as a function of exact cluster size and composition.[23]

At the same time, the details of hydration of acids and bases has been a topic of intense interest in the last decades.[45-52] Cluster studies have permitted the structural and energetic analysis of microsolvated ions, which typically feature only an incomplete first or second solvation shell.[49, 52-54] In particular, photoelectron and vibrational spectroscopies have been applied to clusters of relevance to the atmosphere.[47, 51, 55-58] These studies have established the essential binding motifs of water to cations and anions, with water oxygens bound to either protic or aprotic cations and anions accepting a hydrogen bond from water OH groups.[59, 60] Of particular interest is understanding the initial steps of dissolution, or at least the creation of so-called solvent-separated ion pairs (SSIPs), in which at least one solvent molecule lies between adjacent cations and anions.[53] These efforts have generally found that water binds in motifs that are essentially a superposition of cation and anion hydration structures. Observed formation of SSIPs in ionic clusters has thus far required at least a full coordination shell around the cation, typically an alkali or alkali earth metal, though the formation of an SSIP in hydrated HCl has been suggested to occur with only three or four water molecules present.[61]

Our group recently presented experimentally-derived structures for clusters of ammonia, amines, and sulfuric acid, and developed a simplistic model to predict rough structural features of these clusters.[62] We then used variable-temperature ion traps to establish the compositional and structural dependence of cluster hydration.[63] We hypothesized, from trends in hydration as a function of amine identity, that amine NH groups served as the most likely sites for water binding, and that bisulfate OH groups played a minor secondary role. However, the details of the geometries by which water bound to these clusters could not be determined by mass spectrometry alone. In particular, questions remained about how many hydrogen bonds are involved and whether the water inserted between two ions, as has been found in the case of bisulfate-sulfuric acid clusters,[64] or adopted external bridging or bidentate geometries, seen in clusters of sulfate with atomic cations.[49, 53] In this paper, we present vibrational spectra of these hydrates and propose the water structural motifs to test our hypothesis. We focus on clusters of three ammonium or aminium ions and two bisulfate ions, as these were the topic of our previous report. While the relative contribution of neutral and ionic clusters to NPF remains a topic of intense study,[23, 65] this particular cationic cluster is commonly observed in positive mode electrospray ionization and chemical ionization mass spectrometry, where it has been predicted to be the most stable cationic cluster with two sulfuric acids, and in ambient sampling mass spectrometry in atmospheric simulation experiments.[18, 27, 66, 67]

II. Experimental Procedure

II.1. Experimental Details

All experiments were carried out on a home-built tandem-ion-trap tandem-time-of-flight photofragment mass spectrometer broadly similar to two already described.[68, 69] Briefly, ions are generated in an electrospray ionization (ESI) source housed in an isolated volume that is purged with dry and CO_2-free air or N_2 gas. Here a solution of ammonium bisulfate (1 mM in 50/50 H_2O/MeOH with 0.01% formic acid by volume) was sprayed from a 30 μm diameter fused silica emitter. Clusters containing dimethylamine (DMA) were produced by adding gaseous DMA into the chamber, which led to efficient exchange of ammonia in the as-produced clusters. These ions were sampled into a vacuum system and transported by a series of ion guides to an octopole ion trap attached to a liquid nitrogen cryocooler, capable of operation between 90 and 310 K. Here the ions were exposed to water vapor seeded into helium buffer gas and introduced through a pulsed valve. For the experiments here, this trap was held anywhere between 165 and 190 K depending on the extent of hydration desired. Though we did not specifically test it, it appears that the hydrate distribution roughly reaches equilibrium at a given temperature. A fraction of the ions in this trap are extracted and guided to a second octopole ion trap mounted to a closed-cycle cryocooler operating between 3 and 310 K. At 20 K, this trap yields cold, hydrated complexes with no tags, while reduction of the temperature to 13 K yields D_2-tagged clusters and an increase to 23 K yields N_2-tagged clusters.

With the desired cluster composition is achieved, a fraction of these ions are extracted into an orthogonal acceleration tandem time-of-flight mass spectrometer consisting of a linear stage and a reflectron. At the first time focus, the mass of interest intersected by a pulse from an Nd:YAG-pumped infrared OPO/OPA system (LaserVision). Photofragments (loss of water or N_2) formed at this point are separated from the parent ions in the reflectron analyzer. The output of a microchannel plate detector is amplified and digitized, and the parent and fragment ion intensities are recorded by boxcar averaging these peaks. Laser pulse energies are detected by measuring the energy of a back reflection off the KBr vacuum window with a pyroelectric energy meter whose output is also digitized on every experimental cycle. Spectra are produced by dividing the fragment yield by the sum of the parent and fragment intensities, then further divided by laser

pulse energy to normalize for changes in the laser power as a function of wavelength. These data points are then binned into 1 cm^{-1} bins to produce the final spectra. Laser power is reduced to prevent multiple photofragmentation channels and to avoid suppression of signal due to substantial loss of parent ions, ensuring a nearly linear spectrum.

II.2. Computational Details

All quantum chemical calculations were carried out using the Gaussian 16 suite of programs,[70] with the WebMO interface[71] used to prepare input files and analyze results. Geometries of the dry clusters were previously determined,[72] and hydrate and tag geometries were developed from a combination of exhaustive enumeration and chemical intuition. All spectra were computed at the B3LYP/aug-cc-pVDZ level of theory, which has been shown to produce reasonable agreement with experimental spectra and is computationally efficient enough to permit thorough conformational searches for each hydrate. All computed vibrational spectra are scaled by 0.97, which gave a reasonable qualitative match to the experimental bisulfate OH stretching peak.

III. Results and Discussion

We first will discuss the effect of tag identity on the spectrum in the OH and NH stretching regions, as the binding of a tag induces shifts of bands of the dry cluster associated with the site on which it binds into spectroscopically relevant regions of the spectrum. Next, we will qualitatively analyze the changes in the spectrum upon sequential hydration with an eye towards understanding the gross structural features of the cluster. With this accomplished, we turn our attention to more direct structural determination by comparison of these spectra with predictions from quantum chemical calculations. In the discussion below, we will use the notation (3,2) to denote the cluster $(NH_4^+)_3(HSO_4^-)_2$, the primary focus of this work, and $(3,0,2)_{DMA}$ for dimethylamine containing cluster $((CH_3)_2NH_2^+)_3(NH_4^+)_0(HSO_4^-)_2$, in keeping with our previous naming scheme.

In this manuscript we present spectra recorded using two different infrared action spectroscopy techniques. To avoid confusion on terminology, we will use the term infrared multiple photon dissociation (IRMPD) to denote spectra recorded by monitoring the loss of water, whether this occurs by a single or multiple photon process. It appears that clusters with three or four water molecules feature water bound by an energy of less than a photon at the photon energies used in this study. For spectra recorded by monitoring loss of a tag molecule, we will use the term cryogenic ion vibrational predissociation (CIVP). Comparison of these two techniques identifies the spectral perturbations induced by the tag molecule in CIVP spectroscopy, or the potential intensity uncertainties resulting from the multiple photon process inherent to IRMPD spectroscopy.

III.1. Spectra of Dry Clusters and Tag Effects

It is well established that tag binding induces a red shift of local oscillators in the vicinity of the tag, and potentially shifts in other modes due to other factors such as symmetry breaking, for example.[73, 74] In the case of the clusters studied here, the likely tag binding sites are free NH and OH groups, so tag-induced shifts, if left unassigned, may lead to difficulty in firmly assigning peaks for hydrogen-bonded waters. To this end, we compare in Figure 1 the spectra of bare (3,2) and $(3,0,2)_{DMA}$ clusters in IRMPD (loss of NH_3) or CIVP (with D_2 or N_2 tags) in the free NH and OH stretching regions. No IRMPD yield was detected for the $(3,0,2)_{DMA}$ cluster, which has an expected binding energy for DMA of >40 kcal/mol, requiring several photons at this photon energy. The IRMPD spectrum shows three dominant features, a free OH stretch at 3623 cm^{-1} and NH_2

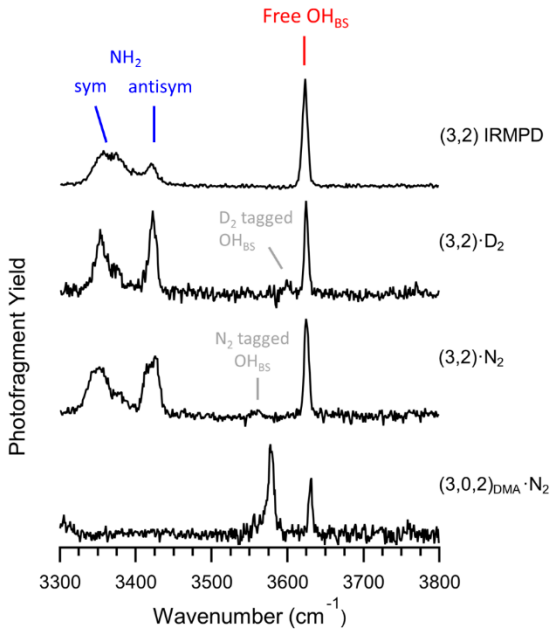

Figure 1: IRMPD spectra of bare (3,2) and CIVP spectra of singly D_2 or N_2 tagged (0,3,2) and singly N_2 tagged $(3,0,2)_{DMA}$. New peaks red shifted from the OH stretch arise due to a fraction of the tag population binding to a bisulfate OH. For the $(3,0,2)_{DMA}$·N_2 spectrum there is no free NH for N_2 to bind to, giving the full intensity of the tag-shifted OH stretch.

symmetric and antisymmetric stretches between 3325 and 3425 cm^{-1}, as previously assigned.[62] The NH_2 symmetric stretch appears as a broad peak split with approximately even intensities between two prominences. This splitting is also been seen in the D_2 and N_2 spectra. Previously assumed to be the result of tag binding to the NH_2, we now tentatively assign the higher energy peak in this feature to an overtone of the NH_4^+ scissors mode that was observed at 1682 cm^{-1} borrowing intensity from the NH_2 symmetric stretch. Upon D_2 complexation, the only qualitative change in the spectrum is the appearance of a weak peak 25 cm^{-1} to the red of the free bisulfate OH, which we assign to the D_2-bound OH stretch. N_2 complexation yields a shift of 64 cm^{-1}, with a concomitant broadening of the NH_2 symmetric and antisymmetric stretching features. Both spectra also reproduce the third feature in the NH stretching manifold, in essentially the same location but with markedly lower intensity. Finally, in the $(3,0,2)_{DMA}$ cluster, there are no NH groups available for tag binding, leaving one free OH as the only possible site for N_2. An intense feature, redshifted by 56 cm^{-1}, is found in the same vicinity as in the spectrum of the N_2-tagged (3,2) cluster.

Taken together, these observations suggest that the most probable tag binding location is the free NH, with the bisulfate OH playing only a minor role, and that the tag-induced effect on the NH stretches is mild. Given that no other tag binding site is available for the $(3,0,2)_{DMA}$ cluster, the intensity of the tagged OH stretch can be assumed to be the innate intensity of this vibration. The intensity of the (3,2) tag-bound OH stretches is around one tenth of this peak. Notably, the tag-shifted peak of doubly-D_2-tagged (3,2) was seen to be approximately twice as intense as the free OH stretch in previous reports.[62] Furthermore, the NH stretching peaks in the D_2-tagged spectra are significantly narrower than those of the N_2-tagged cluster, with the antisymmetric stretch nearly split into two peaks but with a maximum shift of less than 15 cm^{-1}.

III.2. Survey of Spectra of Sequentially-Hydrated Clusters

With the tag effects for the dry clusters characterized, we next turn our attention to the hydrated clusters. The left side of Figure 2 presents IRMPD spectra for the (3,2) cluster with 0-4 water molecules bound, where the dissociation channel for the (3,2) cluster is loss of ammonia and for all hydrates is loss of water. No competitive ammonia loss channel for any hydrate is observed, and the spectra for the third and fourth hydrate appear to occur by absorption of a single photon in this photon energy range, as loss of one and two water molecules are observed in parallel to vary similarly in intensity as the laser power is reduced. This hypothesis is supported by the computed water binding energies, given in Supplemental Information, which are ~90 kJ/mol for the first hydrate, ~45 kJ/mol for the second, and ~40 kJ/mol for the third and fourth. The right side of Figure 2 presents CIVP spectra of N_2-tagged (3,2) clusters with 0-3 water molecules for

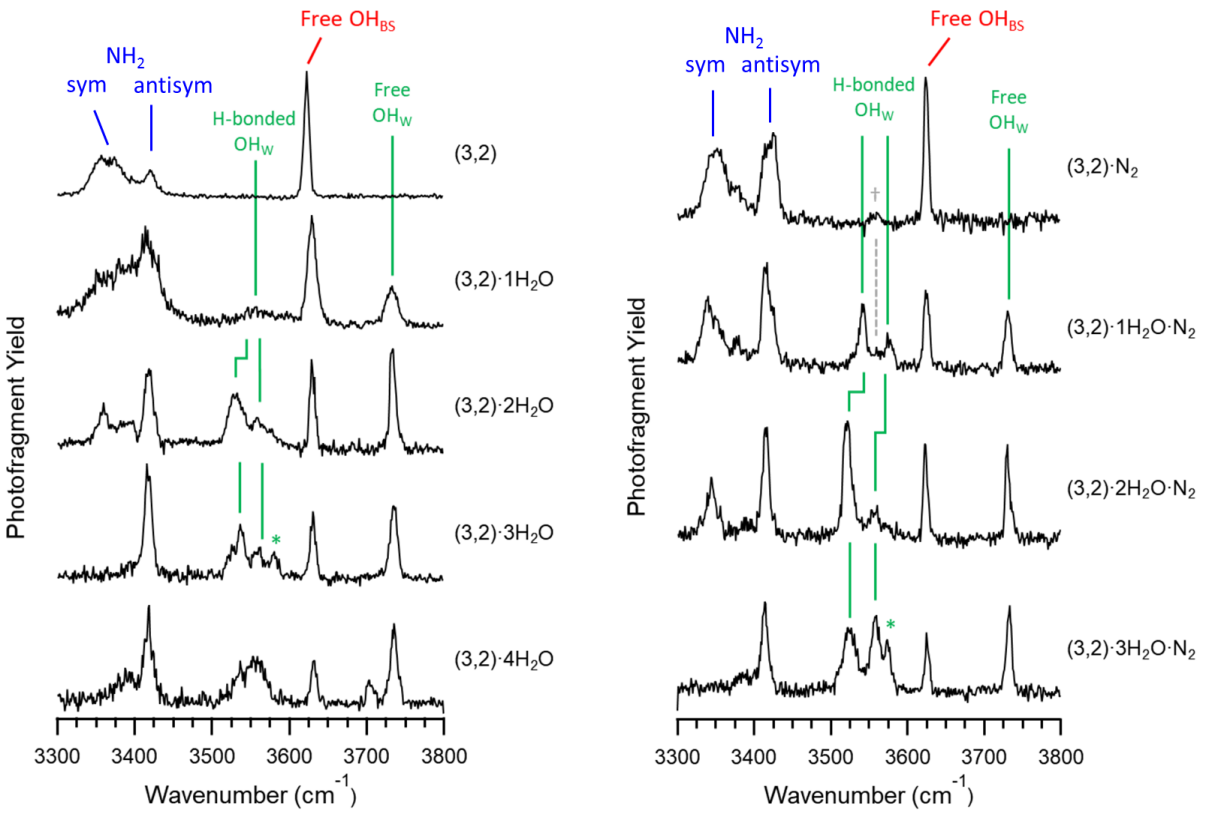

Figure 2: (Left) IRMPD spectra of (3,2) clusters with 0-4 water molecules bound. New features arising from water binding are denoted in green. The higher energy peak is attributed to the free OH stretch of water, while the lower energy features reflect vibrations of the hydrogen-bonded OH. (Right) CIVP spectra of (3,2) clusters with 0-3 water molecules bound. The primary difference is an increase in intensity and resolution for the H-bonded water OH stretches for one water, and an increase in resolution for the same bands in the two water spectrum.

comparison to the IRMPD results. While the spectra are qualitatively similar, some differences in the spectra of the first and second hydrates are apparent, and will be discussed in detail below.

Addition of a single water molecule induces three changes in the IRMPD spectra - a relatively narrow new peak at 3731 cm^{-1}, a new broad feature near 3550 cm^{-1}, and a significant perturbation to the NH_2 stretching region. The CIVP spectra reproduce the high-energy peak, reveal a complex doublet where the broad feature exists in the IRMPD spectrum, and display minimal perturbation to the NH_2 stretching region. The absorption between the two major peaks in the doublet arises in at the same position and with similar intensity to the tag-shifted bisulfate OH and is tentatively assigned to it, suggesting that the primary character of this feature is two peaks separated by 33 cm^{-1}. Given their positions relative to the high-energy stretch and the bisulfate OH stretch, these features are assigned to hydrogen-bonded water OH stretches, while the highest energy feature is assigned to a free water OH stretch. Similar assignments have been proposed for several microhydrated clusters featuring alkali earth cations and conjugate base anions with water molecules solvating the cation and donating a hydrogen bond to the anion.[48, 49, 53] The observation of two hydrogen-bonded OH stretches suggests the presence of at least two isomers and will be discussed in more detail below. An alternative explanation, that one of these peaks is an additional tag-induced red shift of the bisulfate OH, is excluded by $H_2{}^{18}O$-bound spectra shown in the Supporting Information, which show equal shifts for both peaks.

The IRMPD and CIVP spectra of the second hydrate are quite similar to the first, with the notable exception of a ~20 cm^{-1} red shift of both H-bonded OH stretches. The integrated intensity in this region of the IRMPD spectrum of the second hydrate is substantially higher than the first, which suggests increased photodissociation efficiency for this vibration in the second hydrate. Addition of a third water yields substantial differences from the second hydrate but very similar IRMPD and CIVP spectra. Most obviously, the NH stretching region contains only one feature, in the vicinity of the NH_2 antisymmetric stretch in the smaller hydrates. This indicates that each ammonium is H-bonded to exactly one water molecule, leaving one free NH group per ammonium. In addition, the H-bonded OH stretching region now shows three peaks in both spectra, with strikingly similar patterns. The free OH stretching region remains essentially unchanged save a small increase in relative intensity for the highest energy free OH stretch. Finally, addition of a fourth water yields a new peak to the lower energy side of the water free OH stretch and an essentially featureless H-bonded OH stretching region. The new peak in the free OH stretching region suggests that the fourth water molecule binds in a dissimilar motif to the first three, though the exact manner is not clear by inspection of the spectra.

While this qualitative analysis provides gross structural insight, further refinement can be achieved. In the following sections, we discuss more detailed structural aspects of hydration of this cluster by chemical derivatization, isotope exchange, and comparison to quantum chemical predictions. The goal of this analysis is to provide detailed assignment of the potential hydrogen bond donors and acceptors mediating water binding, the order of preference of binding sites, and the potential for co-existing isomers.

III.3. Structural Analysis of Clusters with One Water

Three binding motifs are possible for one molecule on the (3,2) cluster. Water oxygen could hydrogen bond to one of six free NH moieties, one of two free OH moieties, or it could insert between ammonium and bisulfate in six equivalent locations. We first consider the case of water binding to the bisulfate OH. The spectral signature of the OH-bound water can be obtained from the spectrum of the hydrated $(3,0,2)_{DMA}$ cluster, which features no free NH groups and thus will force either the OH-bound or insertion motif. Figure 3 shows the IRMPD spectrum of this cluster along with a quantum chemical prediction and the corresponding minimized structure. This spectrum features two new peaks in the free OH stretching region, separated by ~100 cm^{-1} as is typical for free water symmetric and antisymmetric stretches. The higher-energy feature lies 13 cm^{-1} higher in energy than the water free OH assigned in the previous section, suggesting that the coexistence of a motif with a single free OH like the one in the (3,2) hydrate spectra is unlikely. These features are well-reproduced in the computed spectrum and are not found in the $(3,2)\cdot H_2O$ spectrum.

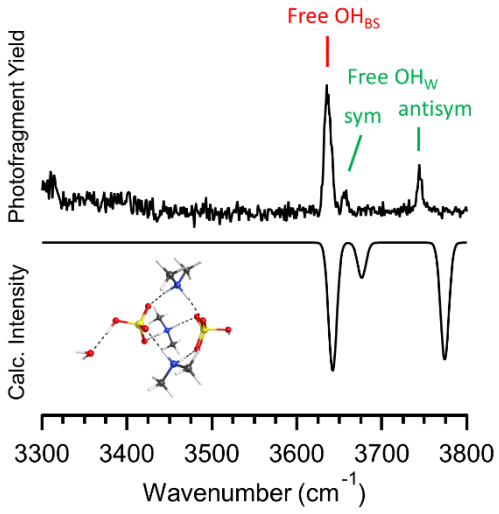

Figure 3: Comparison of the IRMPD and calculated spectra of $(3,0,2)_{DMA}\cdot 1H_2O$, where the water is bound to the bisulfate OH with both water OH groups free. Inset is the calculated structure for this arrangement.

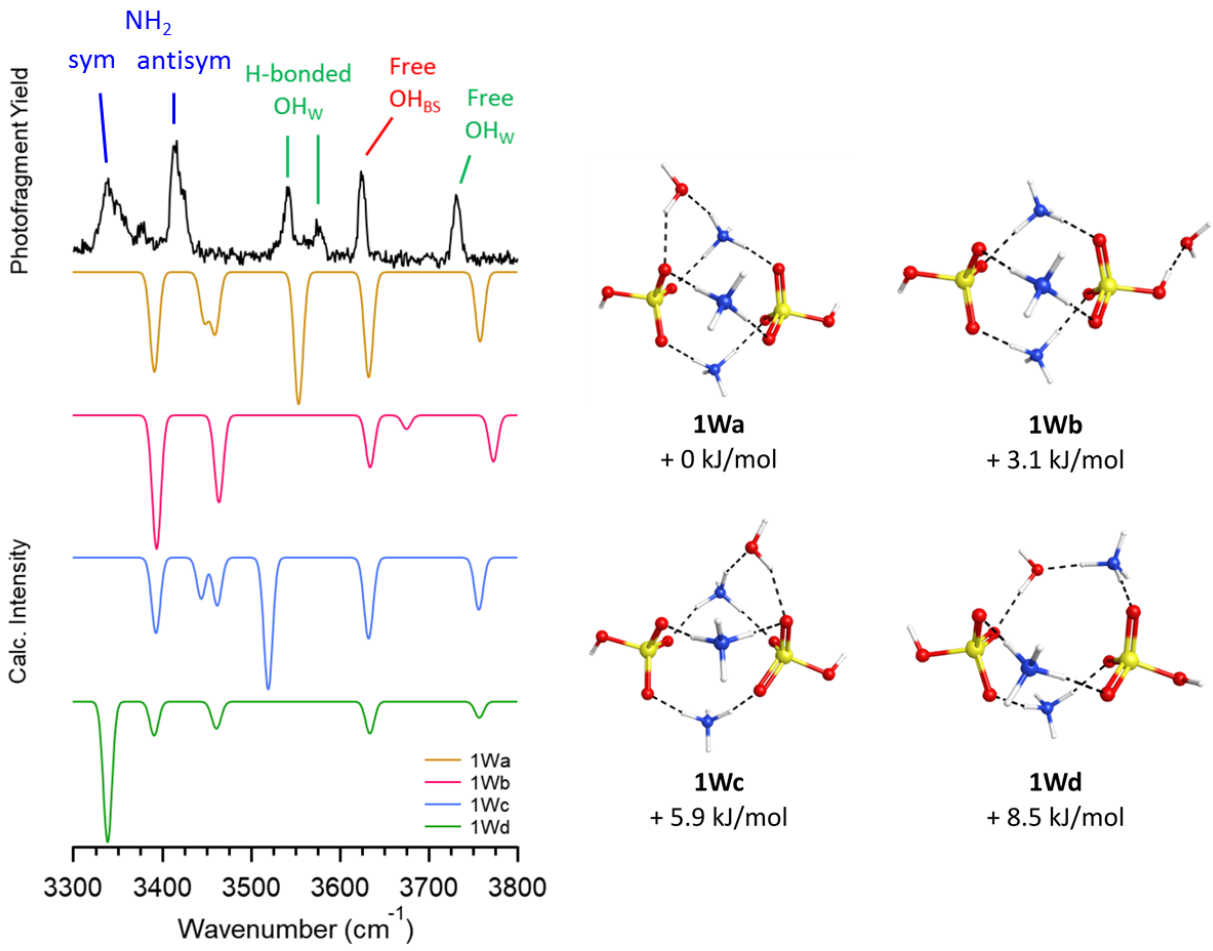

Figure 4: Comparison between N_2 tagged spectrum of (3,2)·1H_2O and calculated spectra for four low-lying isomers. Included to the right are the computed structures for these isomers and their relative zero-point corrected energies. Three arrangements are possible: water bound to an NH, to an OH, or inserted between an ammonium and bisulfate.

The CIVP spectrum of (3,2)·H_2O·N_2 is reproduced in Figure 4, and compared to computed spectra for four different cluster geometries. After scaling the computed frequencies to bring the bisulfate OH stretching frequencies into near agreement, the computed NH stretches can be seen to lie higher in energy than the corresponding experimental features. This was previously observed for ammonium bisulfate clusters in calculations using B3LYP-based methods, however the overall success of this computational method in predicting the full spectra reported for those clusters justified their use over alternate functionals.[72] The bisulfate OH-bound water is the second lowest energy structure found (labeled 1Wb), but the experimental spectrum does not show the free water symmetric and antisymmetric stretches as outlined for the $(3,0,2)_{DMA}$ cluster above, indicating that this isomer is not present. Next we consider the arrangement in which water inserts between the cation and anion. In this case (1Wd), the spectrum would be expected to display a free OH stretch and an H-bonded stretch that is substantially red shifted due to the strong single-donor-single-acceptor ionic hydrogen bond, as well as a notable difference in the NH stretching region. While this arrangement suffers a Coulombic energy penalty, this may be offset by the formation of an additional strong hydrogen bond or proton transfer. Indeed, the zero-point corrected internal energy of this arrangement is found to be 8.5 kJ/mol higher than the lowest energy structure sampled. However, the predicted spectrum for this structure shows the H-bonded OH stretch shifted to lower energy than the NH stretches, and given its likely high anharmonicity, the experimental peak location can be expected to be to the red of the harmonic

prediction. It does not account for the H-bonded OH stretches, either, so it could certainly not be the only isomer present.

The final binding motif under consideration is water bound to a free NH. If the water is only bound to an NH, this arrangement could be expected to yield symmetric and antisymmetric water stretches similar to those for the OH-bound configuration. However, calculations beginning with this geometry optimize to the substantially more stable cyclic arrangement, in which one water OH donates a hydrogen bond to a bisulfate SO as shown in structures 1Wa and 1Wc. In this scenario, two isomers are found. A minimally-perturbative structure in which the water spans the helical H-bonding network, which we denote "staggered" to represent the relative orientations of the bisulfate SO_3 groups, involves minimal rearrangement of the cluster structure to accommodate the incoming water. Another, denoted "eclipsed", in which the water binds in an opposite helicity, substantially disrupting the structure. Surprisingly, this structure is computed to lie only 5.9 kJ/mol above the less disruptive one. As evidenced in the computed spectra, the difference between the H-bonded OH stretches is predicted to be very similar to the difference between the experimental peaks, but the computed peaks appear at significantly lower energy. In addition, the eclipsed arrangement in 1Wc features a significant split of the NH_2 antisymmetric stretches that is not found in the experimental spectrum. An alternate hypothesis is that one of the two peaks is a tag effect, but the IRMPD spectrum of the $H_2{}^{18}O$ hydrate features two similar peaks (shown in Supporting Information), suggesting that these peaks do not arise from tag effects. The two peaks shift similarly under $H_2{}^{18}O$ substitution in CIVP spectra, which is inconsistent with, but does not rule out, anharmonic effects such as Fermi resonances. A final possibility is that the lower energy of the two peaks is attributed to the staggered isomer, while the higher energy should be ascribed to an as-yet-unidentified isomer. While the precise geometry remains unclear, the assignment of the structure to NH bound water appears firm, particularly in light of the above-mentioned observation that upon binding of a third water, each ammonium ion features exactly one bound water.

III.4. Structural Analysis of Clusters with Two Waters

Figure 5 presents the experimental CIVP spectrum for $(3,2)\cdot 2H_2O\cdot N_2$ along with predicted spectra for selected low-energy isomers. The significant similarity between the spectra for clusters featuring one and two waters suggests a broadly similar binding motif. At first glance, it appears that the two H-bonded OH stretching peaks from the first hydrate have slightly red shifted upon the addition of a second water. In addition, in both the IRMPD and CIVP spectra the higher energy feature appears substantially broader than the lower energy feature, or either feature in the CIVP spectrum of the single hydrate. This is likely due to the onset of modulation of the OH stretching frequency by large amplitude motion of low-energy vibrations, which has been seen in spectra of microsolvated salt clusters with water in bridging arrangements.[48, 53] Beyond these changes, the only shift greater than 1 cm^{-1} observed in the CIVP spectrum of the second hydrate is the 4 cm^{-1} blue shift of the NH_2 symmetric stretching vibration. Given these observations, we conclude that no major differences exist between water binding motifs of the first and second water molecule.
Since the first water breaks the symmetry of the cluster, not all free NH or OH moieties are identical. Ruling out the OH binding and insertion structures as for the first water, the second water molecule finds, to a rough approximation, two potentially favorable binding sites: a free NH on one of the two ammonium ions without water, or the remaining free NH of the ammonium to which the first water is bound. These two possibilities cannot be separated by inspection of the experimental spectrum alone, so we again turn to computed spectra to aid in structural assignment. We first see that the spectrum for the case when both water molecules are bound to a single ammonium ion (2Wf) displays clear changes in the free water OH stretching and the ammonium symmetric and antisymmetric stretching vibrations that are not observed in the

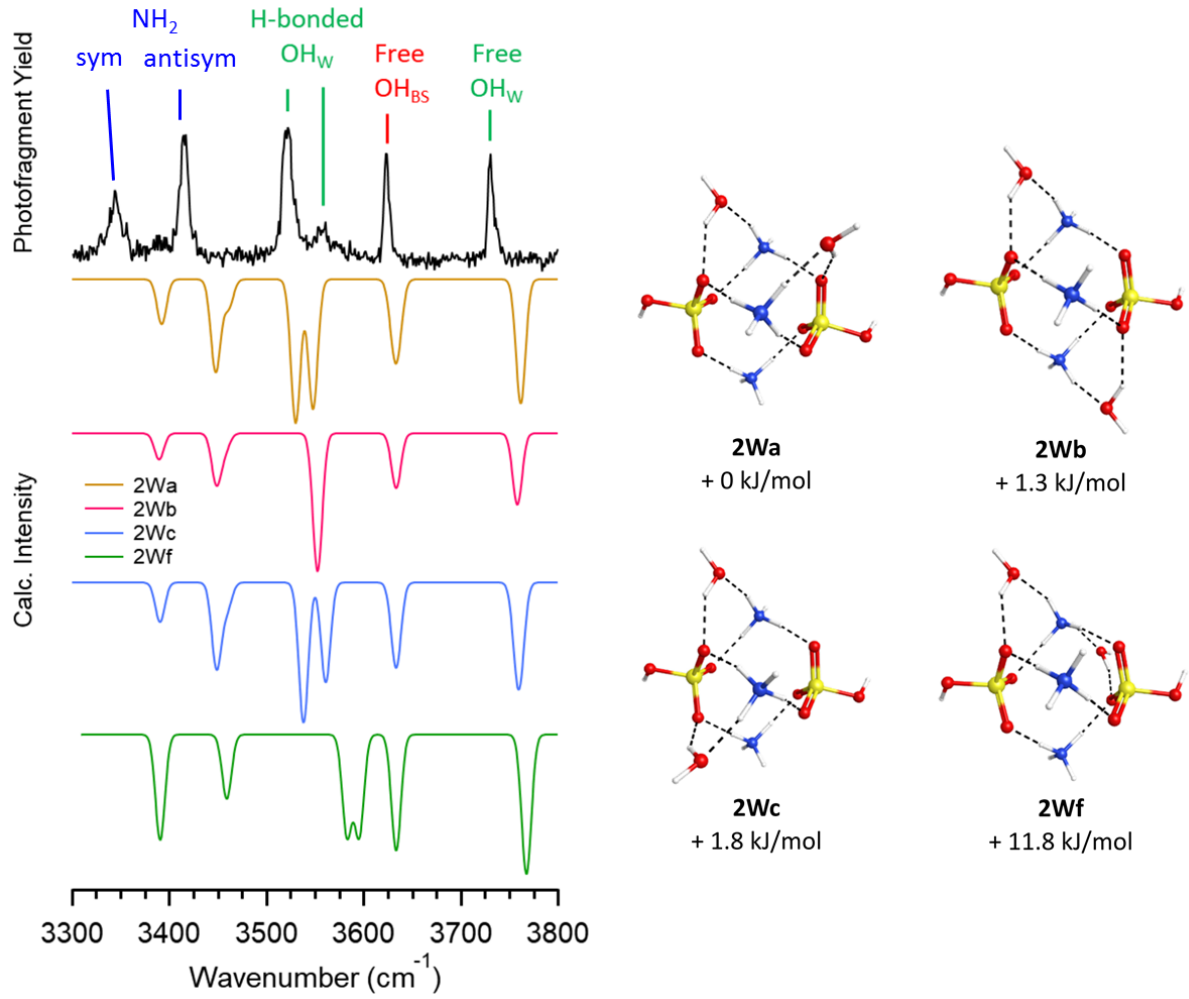

Figure 5: Comparison of the N_2 tagged spectrum of (3,2)·2H_2O to calculated spectra of selected low-lying isomers. For 2Wa, b, and c, waters are bound to different ammonium ions, where 2Wf has both waters bound to the same ammonium, leading to substantial changes in intensity for the NH stretches and a smaller red shift of the H-bonded OH stretch.

experimental spectrum. This, combined with the prediction of H-bonded water OH stretches at energies not reproduced in the experimental spectrum, leads us to conclude that this arrangement is not present.

In the case that both water molecules reside on different ammonium ions, still not all binding sites are exactly equal. Three isomers with nearly isoenergetic internal energies are presented for cases where each water binds to a different ammonium (2Wa-c). In 2Wc, the second water donates a proton to the same bisulfate as the first one, while in 2Wa and 2Wb, the second water is on the opposite side of the cluster. For the latter cases, the water molecules can take on two relative arrangements, one in which the second water binds to the nearest NH such that the two H-bonded OH bonds are nearly antiparallel, and another in which the second water binds to the farther NH, which leads to a nearly perpendicular alignment for these two OH bonds. As can be seen in the computed spectra, these three isomers display essentially identical spectra for the water free OH and NH_2 stretches, with the only notable differences occurring in the H-bonded OH stretches. None of the H-bonded stretches match the experimental features particularly well, but they all fall in the range of the experimental peaks and they are calculated to lie within 1.8 kJ/mol of each other. This is well within the expected uncertainty of the quantum chemical method

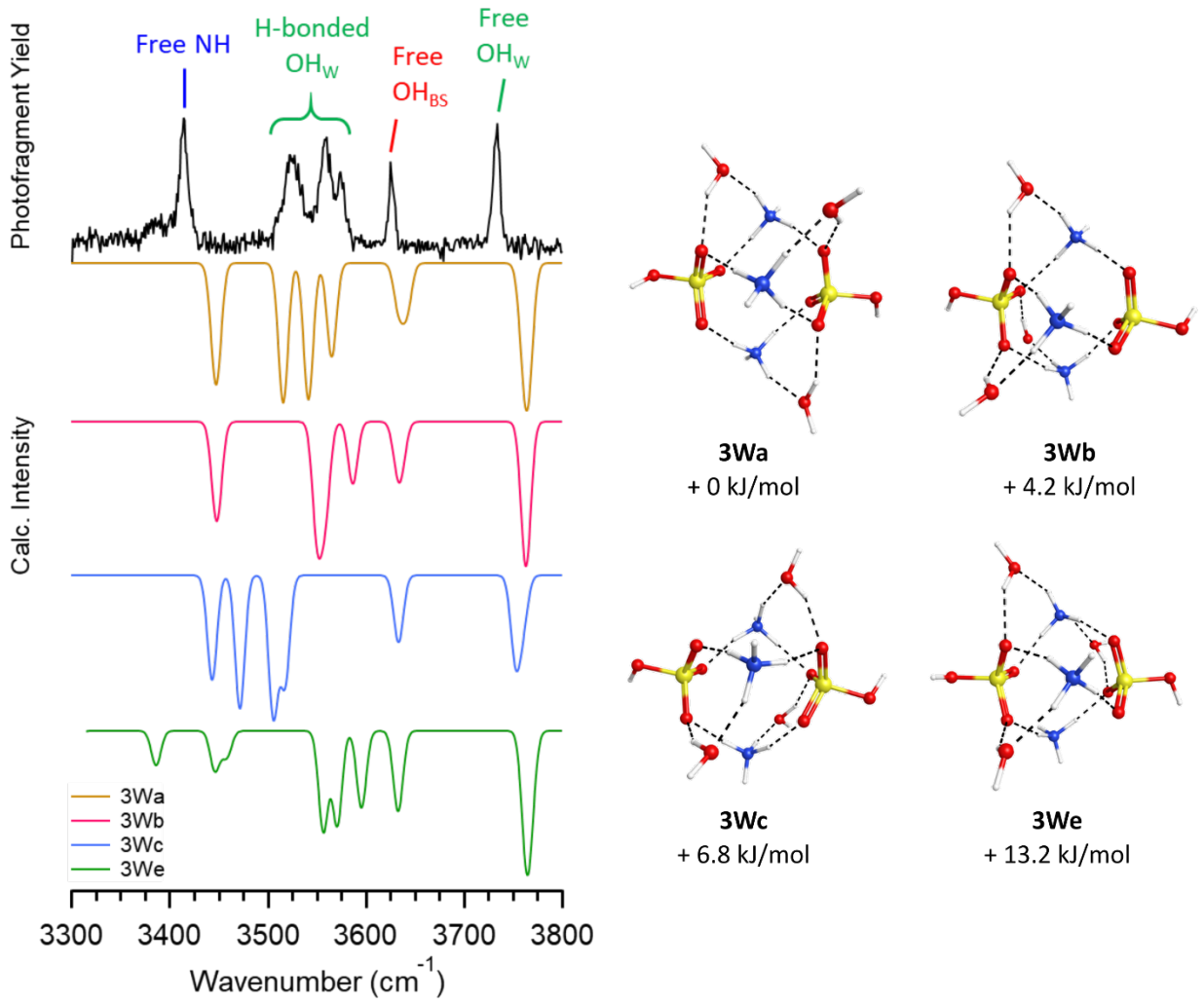

Figure 6: Comparison of the N_2 tagged spectrum of (3,2)·3H_2O to calculated spectra for several low-lying isomers. The 3We structure features one ammonium with two water molecules bound and one with zero, giving rise to NH_2 symmetric and antisymmetric features not seen in the experimental spectrum.

employed here, and is significantly lower than thermal energy at atmospheric conditions, suggesting that any of these isomers could be populated in atmospheric conditions. Of the three, 2Wc best reproduces the splitting between the two peaks, and the difference in relative intensities could be explained by a significantly broader higher-energy peak. Analysis of these peaks shows that the splitting arises from the fact that one water donates a hydrogen bond to the same SO as an ammonium bound to the other water, while the second water donates a hydrogen bond to an SO that is shared with a bare ammonium ion. While not definitive as to the absolute geometry, the assignment of the general motif, like in the case of the single water clusters, is firm.

III.5. Structural Analysis of Clusters with Three Waters

Much like the case of the double hydrates, the third water molecule also could find both free NH and NH_2 binding sites. However, the gross structural assignment for this clusters is much simpler, as the NH_2 stretching region, reproduced in Figure 6 along with computed spectra, collapses into a single, relatively sharp strong feature with a low-intensity shoulder at lower energy. From this observation, we conclude that each ammonium binds one water molecule, leaving three

degenerate or nearly-degenerate free NH stretches. Both free water and bisulfate OH stretches remain unchanged, save for an increase in the relative intensity of the water free OH stretch that is ascribed to the addition of a third contribution to the peak. The H-bonded OH stretches are split into a triplet, which is consistent between CIVP and IRMPD spectra. From these similarities alone, we can rule out possibilities in which water binds to a bisulfate OH, inserts into the cluster, or binds to an NH of an ammonium that already has a water bound to it. The remaining question is whether all water molecules are interacting with the same bisulfate, or rather one is on the other side of the cluster.

The computed spectra for the low-lying isomers with this configuration again display very similar free OH and NH stretching peaks, differing only in the H-bonded OH stretching region. The eclipsed geometry (3Wc) produces a peak lower in energy than the experimental feature, while 3Wa and 3Wb produce peaks in the vicinity of the experimental peaks. The case in which one water binds to the bisulfate on the opposite side of the cluster produces three peaks with spacing similar to that observed in the experiment and lies 4.2 kcal/mol lower in energy, suggesting that this is the most probable isomer in atmospheric conditions. In our experiment, water molecules are likely to be added to the cluster sequentially. Notably, this cluster structure represents a combination of the three lowest-lying isomers for the double hydrate, suggesting that water uptake to this structure is also combinatorially favorable. The 3Wb structure can only be reached either by addition of water to the 2Wc structure or by rearrangement from 3Wa, making this structure less favorable in the growth process.

III.6. Structural Analysis of Clusters with Four Waters

Addition of the fourth water presents an interesting question: with all three ammonium ions singly hydrated, is it preferred to produce a doubly-hydrated ammonium or is the bisulfate OH the next best site? As mentioned in Section III.2, the primary spectral change upon incorporation of the fourth water is a new peak just to the red of the free water OH stretch, along with broadening in the H-bonded OH stretching region. We rule out the possibility of a free water bound to the bisulfate OH because this spectrum is dissimilar to the $(3,0,2)_{DMA}$ one. This leaves two likely binding motifs: the fourth water bound to one of the three remaining NH hydrogens, forming an ammonium with two bound water molecules, or bound to a bisulfate OH with a secondary hydrogen bond to one of the first three water molecules. An arrangement such as this would explain both the broadening of the H-bonded OH stretching region and the new free OH stretching peak appearing to the red of the previous one. A final possibility is that three water molecules are enough to solvate an ion, making it more favorable to insert water between an ammonium and a bisulfate.

Figure 7 gives the IRMPD spectrum of $(3,2)\cdot 4H_2O$ and selected computed spectra for several isomers. Four isomers (4Wa-d) were found that feature water in very similar arrangements, based off of hydrating one of the three low-lying isomers for the third hydrate, and thus only the lowest-energy isomer is presented here. All isomers are included in the Supporting Information. In this class of isomers, water is bound to the bisulfate OH and one of the water molecules previously identified above. The next higher energy class of isomers features a water molecule inserted between a cation and anion, followed by water on a free bisulfate OH without a secondary hydrogen bond, and finally, two water molecules bound the same ammonium ion. Comparison to the computed spectra shows that only the first class of structures are able to reproduce the new free OH stretch. The lowest-energy computed transition is linked to the water-water H-bonded stretch, and is likely significantly red shifted in the experimental spectrum. The broadening of the H-bonded stretching region in this cluster is often seen upon the formation of incipient water networks in hydrated ionic clusters, and has been ascribed to the onset of large-amplitude motion

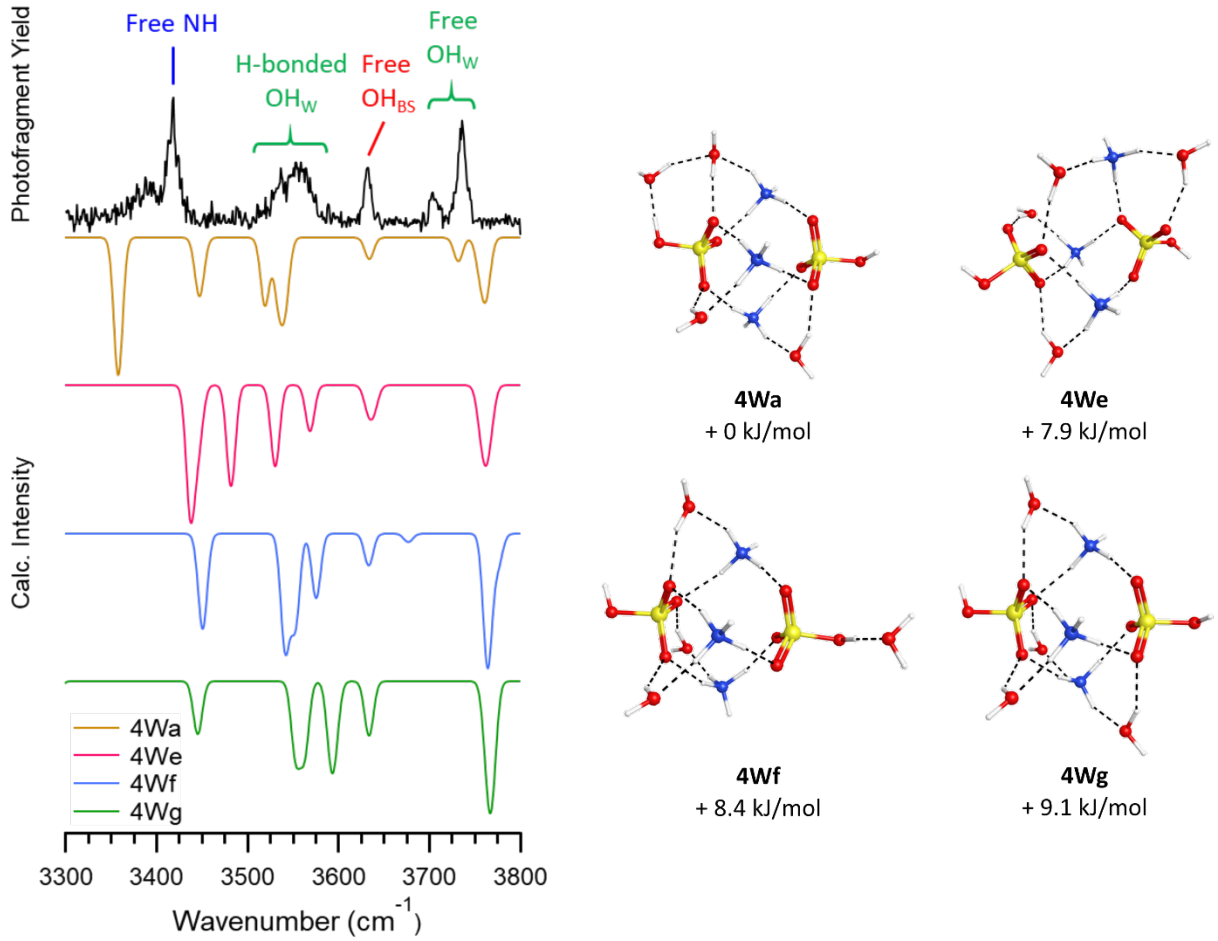

Figure 7: Comparison of the IRMPD spectrum of (3,2)·4H_2O to calculated spectra for several low lying isomers. The 4Wb, c, and d structures are broadly similar and give similar computed spectra, so they are not included here.

that modulates the H-bonded OH stretching frequencies even at the zero-point level. This impedes the assignment of peaks in this area, and thus it is sufficient to find harmonic predictions in the general energy range of the broad feature. As with the third hydrate, the fourth water can grow through pathways requiring minimal rearrangement for addition of one water to any of the low-lying triple hydrate structures.

III.7. General Discussion of Ammonium Bisulfate Cluster Hydration

Given the structural analysis outlined above, we turn to a discussion of the insight gleaned for ammonium bisulfate hydration. As proposed from our previous mass spectral data, and consistent with several calculations of hydrated neutral clusters,[28, 40, 41] we find that ammonium ions are the most likely binding sites for water molecules. The current spectroscopy results further clarify this observation: water first binds to free NH_2 groups preferentially, and only after that to a bisulfate OH. Once each ammonium binds one water molecule, its second binding site is apparently less favorable than the bisulfate free OH, despite the fact that in both cases a bound water can form a second hydrogen bond to become further stabilized. This suggests that, in the atmosphere, cluster hydration is likely well-estimated by the number of surface NH groups in the vicinity of a hydrogen bond accepting group such as an S=O, and thus clusters with more ammonia content are more likely to be hydrated than clusters composed primarily of sulfuric acid. Due to the specific

geometry of the hydrates, water binding at this site is able to form a secondary hydrogen bond with one of the ammonium-bound waters in a cyclic arrangement, potentially foretelling the formation an incipient water hydrogen bonding network patterned by the cluster anions and cations. However, given that these clusters are only expected to feature a few water molecules in the ambient atmosphere,[40, 63] this network is unlikely to extend into a second solvation shell.

The sequential addition of water to these clusters in our experiment enforces a mechanistic pathway on the hydrate structures. If a low-energy isomer for a higher hydrate requires a substantial rearrangement of the lower hydrate, this pathway may be blocked both in our experiment and in ambient conditions. In all structures studied here, the lowest energy class of isomers for each hydration number can be explained by simple addition of water to the lower hydrate, suggesting that any barriers necessary to be overcome are low or nonexistent. The fact that computed structures show a slight preference for water binding on opposite sides of the cluster indicates that much more water may be necessary to "dissolve" the cluster to form solvent-separated ion pairs. The experiments here are carried out here produce a distribution of hydrates peaked in the range of 1-4, which can be controlled by varying the temperature over the range 160-190 K. Theoretical efforts suggest that, in atmospheric conditions, these clusters will not be substantially more hydrated,[23, 40] and thus we suspect that bound waters will remain on the cluster surface and the core will remain salty for clusters of this type forming in the ambient atmosphere. This observation suggests a core-shell model of cluster hydration, in which water mediates surface interactions of condensing vapors but does not qualitatively change the chemistry of the cluster core.

The potential contribution of isomers to the cluster structural ensemble is an important question. Current models predicting new particle formation rates in ambient conditions typically assume that a single isomeric species is present, and compute evaporation and condensation rates from heats of formation on that assumption.[21] Explicit incorporation of water into these models is difficult, but the potential presence of equivalent or nearly-equivalent binding sites and hydration isomers may contribute a significant entropic component to these rates, which determine the overall particle formation rates. Our experiments are unable to confirm or rule out the potential role of hydration isomers, and our quantum chemical calculations suggest that for doubly, triply, and quadruply hydrated clusters, several low-lying isomers exist within the window of thermal energy available in ambient conditions. The similarity of the energies of the various isomers for the case of the first three water adducts suggests that multiple similar pathways for hydration of this cluster exist up to three water molecules, after which hydration is more constrained. Future isomer-specific double resonance or hole burning experiments will help to clarify this aspect of the problem. Furthermore, several structures for the higher hydrates can be formed from hydration of multiple different nearly isenthalpic isomers of the lower hydrate, providing an entropic driving force that could potentially overcome small enthalpic differences calculated here. A detailed quantitative analysis of the water uptake or dissociation kinetics, either using the temperature control available in our ion traps or via single-collision threshold collision induced dissociation experiments, could quantify this effect.

Finally, we note that the structural analysis performed here remains largely qualitative. Our priority was first to establish the large-scale structural motifs likely to be involved in hydration of these clusters. While exact structural identification is likely not critical for the purposes of understanding water's impact on the mechanism of NPF, more firm and detailed assignments await the collection of full-range vibrational spectra and improved quantum chemical calculations and configurational searching. In particular, symmetry breaking of the fingerprint vibrations of bisulfate, ammonium, and water can offer further clues for structural assignment and validation for computed spectra. Water and NH_2 bending vibrations, as well as bisulfate SO_3 symmetric stretches and SOH bends,

are sensitive to hydrogen bonding and symmetry breaking. Efforts in our group are underway to extend these results to 600 cm^{-1} to clarify these details.

IV. Conclusions

We have analyzed the binding motifs of water bound to a prototypical cluster containing three ammonium cations and two bisulfate anions using mass-selective vibrational spectroscopy and quantum chemical calculations. We find that ammonium NH groups are the optimal binding sites for the first three water molecules, with each ammonium ion binding only one water molecule. The binding structure is best described as one hydrogen bond between an ammonium NH and the water oxygen and an additional hydrogen bond between a water OH and a bisulfate SO, yielding a bent cyclic structure. The fourth water forms one hydrogen bond between the bisulfate OH and the water oxygen and one more between the OH-bound water OH and the ammonium-bound water oxygen. Within these structural classifications, several potential isomeric structures exist depending on the specific orientation between waters in nominally-identical NH and OH binding sites. In some cases, the computed zero-point corrected electronic energies of these clusters are close enough to suggest that isomers may contribute to hydrate structures in the ambient atmosphere, and the spectroscopic information in these cases does not provide enough information to rule out this possibility. The structures discussed here provide an intuitive pathway to rationalize the stepwise hydration of these clusters, and water uptake can proceed without requiring substantial rearrangement up to at least four water molecules. These observations suggest that entropic contributions from isomers may be significant enough to play a role in the energetics of growth of new particles under conditions in which they are hydrated.

References

1. M. Kulmala, I. Riipinen, M. Sipila, H. E. Manninen, T. Petaja, H. Junninen, M. D. Maso, G. Mordas, A. Mirme, M. Vana, et al., *Science*, 2007, **318**, 89-92.
2. R. Zhang, *Science*, 2010, **328**, 1366-1367.
3. T. Stocker, D. Qin, G. Plattner, M. Tignor, S. Allen, J. Boschung, A. Nauels, Y. Xia, V. Bex and P. Midgley, *IPCC, 2013: Climate Change 2013: The Physical Science Basis. Contribution of Working Group I to the Fifth Assessment Report of the Intergovernmental Panel on Climate Change, 1535 pp*, Cambridge Univ. Press, Cambridge, UK, and New York, 2013.
4. R. C. Sullivan, P. Crippa, H. Matsui, L. R. Leung, C. Zhao, A. Thota and S. C. Pryor, *npj Climate and Atmospheric Science*, 2018, **1**, 9.
5. J. Almeida, S. Schobesberger, A. Kürten, I. K. Ortega, O. Kupiainen-Määttä, A. P. Praplan, A. Adamov, A. Amorim, F. Bianchi, M. Breitenlechner, et al., *Nature*, 2013, **502**, 359-363.
6. F. Riccobono, S. Schobesberger, C. E. Scott, J. Dommen, I. K. Ortega, L. Rondo, J. Almeida, A. Amorim, F. Bianchi, M. Breitenlechner, et al., *Science*, 2014, **344**, 717-721.
7. F. Arnold, A. A. Viggiano and H. Schlager, *Nature*, 1982, **297**, 371.
8. C. A. Brock, P. Hamill, J. C. Wilson, H. H. Jonsson and K. R. Chan, *Science*, 1995, **270**, 1650.
9. Y. Viisanen, M. Kulmala and A. Laaksonen, *J. Chem. Phys.*, 1997, **107**, 920-926.
10. M. Kulmala, A. Laaksonen and L. Pirjola, *J. Geophys. Res: Atmos.*, 1998, **103**, 8301-8307.
11. E. R. Lovejoy, J. Curtius and K. D. Froyd, *J. Geophys. Res: Atmos.*, 2004, **109**, D08204.
12. M. Chen, M. Titcombe, J. Jiang, C. Jen, C. Kuang, M. L. Fischer, F. L. Eisele, J. I. Siepmann, D. R. Hanson, J. Zhao, et al., *Proc. Natl. Acad. Sci.*, 2012, **109**, 18713.
13. M. Kulmala, T. Petäjä, M. Ehn, J. Thornton, M. Sipilä, D. R. Worsnop and V. M. Kerminen, *Annu. Rev. Phys. Chem.*, 2014, **65**, 21-37.
14. K. Lehtipalo, L. Rondo, J. Kontkanen, S. Schobesberger, T. Jokinen, N. Sarnela, A. Kürten, S. Ehrhart, A. Franchin, T. Nieminen, et al., *Nat. Commun.*, 2016, **7**, 11594.
15. L. Yao, O. Garmash, F. Bianchi, J. Zheng, C. Yan, J. Kontkanen, H. Junninen, S. B. Mazon, M. Ehn, P. Paasonen, et al., *Science*, 2018, **361**, 278-281.
16. C. N. Jen, P. H. McMurry and D. R. Hanson, *J. Geophys. Res: Atmos.*, 2014, **119**, 7502-7514.
17. B. Temelso, E. F. Morrison, D. L. Speer, B. C. Cao, N. Appiah-Padi, G. Kim and G. C. Shields, *J. Phys. Chem. A*, 2018, **122**, 1612-1622.
18. F. Bianchi, A. P. Praplan, N. Sarnela, J. Dommen, A. Kürten, I. K. Ortega, S. Schobesberger, H. Junninen, M. Simon, J. Tröstl, et al., *Environ. Sci. Technol.*, 2014, **48**, 13675-13684.
19. E. M. Dunne, H. Gordon, A. Kürten, J. Almeida, J. Duplissy, C. Williamson, I. K. Ortega, K. J. Pringle, A. Adamov, U. Baltensperger, et al., *Science*, 2016, **354**, 1119-1124.
20. S. Schobesberger, H. Junninen, F. Bianchi, G. Lönn, M. Ehn, K. Lehtipalo, J. Dommen, S. Ehrhart, I. K. Ortega, A. Franchin, et al., *Proc. Natl. Acad. Sci.*, 2013, **110**, 17223-17228.
21. M. J. McGrath, T. Olenius, I. K. Ortega, V. Loukonen, P. Paasonen, T. Kurtén, M. Kulmala and H. Vehkamäki, *Atmos. Chem. Phys.*, 2012, **12**, 2345-2355.
22. H. Vehkamaki and I. Riipinen, *Chem. Soc. Rev.*, 2012, **41**, 5160-5173.

23. T. Olenius, R. Halonen, T. Kurtén, H. Henschel, O. Kupiainen-Määttä, I. K. Ortega, C. N. Jen, H. Vehkamäki and I. Riipinen, *J. Geophys. Res: Atmos.*, 2017, **122**, 7103-7118.
24. J. Elm, M. Passananti, T. Kurtén and H. Vehkamäki, *J. Phys. Chem. A*, 2017, **121**, 6155-6164.
25. T. Kurtén, V. Loukonen, H. Vehkamäki and M. Kulmala, *Atmos. Chem. Phys.*, 2008, **8**, 4095-4103.
26. V. Loukonen, T. Kurtén, I. K. Ortega, H. Vehkamäki, A. A. H. Pádua, K. Sellegri and M. Kulmala, *Atmos. Chem. Phys.*, 2010, **10**, 4961-4974.
27. K. D. Froyd and E. R. Lovejoy, *J. Phys. Chem. A*, 2012, **116**, 5886-5899.
28. J. W. DePalma, D. J. Doren and M. V. Johnston, *J. Phys. Chem. A*, 2014, **118**, 5464-5473.
29. N. T. Tsona, H. Henschel, N. Bork, V. Loukonen and H. Vehkamäki, *J. Phys. Chem. A*, 2015, **119**, 9670-9679.
30. B. R. Bzdek, J. W. DePalma and M. V. Johnston, *Acc. Chem. Res.*, 2017, **50**, 1965-1975.
31. C. N. Jen, R. Bachman, J. Zhao, P. H. McMurry and D. R. Hanson, *Geophys. Res. Lett.*, 2015, **43**, 867-873.
32. J. Elm, C. N. Jen, T. Kurtén and H. Vehkamäki, *J. Phys. Chem. A*, 2016, **120**, 3693-3700.
33. R. Zhang, I. Suh, J. Zhao, D. Zhang, E. C. Fortner, X. Tie, L. T. Molina and M. J. Molina, *Science*, 2004, **304**, 1487-1490.
34. J. N. Smith, K. C. Barsanti, H. R. Friedli, M. Ehn, M. Kulmala, D. R. Collins, J. H. Scheckman, B. J. Williams and P. H. McMurry, *Proc. Natl. Acad. Sci.*, 2010, **107**, 6634-6639.
35. I. Riipinen, T. Yli-Juuti, J. R. Pierce, T. Petäjä, D. R. Worsnop, M. Kulmala and N. M. Donahue, *Nat. Geosci.*, 2012, **5**, 453-458.
36. T. Berndt, M. Sipilä, F. Stratmann, T. Petäjä, J. Vanhanen, J. Mikkilä, J. Patokoski, R. Taipale, L. Mauldin III and M. Kulmala, *Atmos. Chem. Phys. Discuss.*, 2013, **13**, 16301-16335.
37. M. L. Dawson, M. E. Varner, V. Perraud, M. J. Ezell, R. B. Gerber and B. J. Finlayson-Pitts, *P. Natl. Acad. Sci. USA*, 2012, **109**, 18719-18724.
38. A. Kürten, C. Li, F. Bianchi, J. Curtius, A. Dias, N. M. Donahue, J. Duplissy, R. C. Flagan, J. Hakala, T. Jokinen, et al., *Atmos. Chem. Phys.*, 2018, **18**, 845-863.
39. K. Lehtipalo, C. Yan, L. Dada, F. Bianchi, M. Xiao, R. Wagner, D. Stolzenburg, L. R. Ahonen, A. Amorim, A. Baccarini, et al., *Science Advances*, 2018, **4**, eaau5363.
40. H. Henschel, J. C. A. Navarro, T. Yli-Juuti, O. Kupiainen-Määttä, T. Olenius, I. K. Ortega, S. L. Clegg, T. Kurtén, I. Riipinen and H. Vehkamäki, *J. Phys. Chem. A*, 2014, **118**, 2599-2611.
41. H. Henschel, T. Kurtén and H. Vehkamäki, *J. Phys. Chem. A*, 2016, **120**, 1886-1896.
42. J. W. DePalma, B. R. Bzdek, D. J. Doren and M. V. Johnston, *J. Phys. Chem. A*, 2012, **116**, 1030-1040.
43. J. V. Kildgaard, K. V. Mikkelsen, M. Bilde and J. Elm, *J. Phys. Chem. A*, 2018, **122**, 5026-5036.
44. J. V. Kildgaard, K. V. Mikkelsen, M. Bilde and J. Elm, *J. Phys. Chem. A*, 2018, **122**, 8549-8556.
45. J. M. Lisy, *Int. Rev. Phys. Chem.*, 1997, **16**, 267-289.
46. J. Zhou, G. Santambrogio, M. Brümmer, D. T. Moore, L. Wöste, G. Meijer, D. M. Neumark and K. R. Asmis, *J. Chem. Phys.*, 2006, **125**, 111102.

47. T. I. Yacovitch, T. Wende, L. Jiang, N. Heine, G. Meijer, D. M. Neumark and K. R. Asmis, *J. Phys. Chem. Lett.*, 2011, **2**, 2135-2140.
48. C. J. Johnson, L. C. Dzugan, A. B. Wolk, C. M. Leavitt, J. A. Fournier, A. B. McCoy and M. A. Johnson, *J. Phys. Chem. A*, 2014, **118**, 7590-7597.
49. T. Wende, N. Heine, T. I. Yacovitch, K. R. Asmis, D. M. Neumark and L. Jiang, *Phys. Chem. Chem. Phys.*, 2016, **18**, 267-277.
50. J. M. Thomas, S. He, C. Larriba-Andaluz, J. W. DePalma, M. V. Johnston and C. J. Hogan Jr., *Phys. Chem. Chem. Phys.*, 2016, **18**, 22962-22972.
51. G.-L. Hou, J. Zhang, M. Valiev and X.-B. Wang, *Phys. Chem. Chem. Phys.*, 2017, **19**, 10676-10684.
52. L. Jiang, T. Wende, R. Bergmann, G. Meijer and K. R. Asmis, *J. Am. Chem. Soc.*, 2010, **132**, 7398-7404.
53. J. W. DePalma, P. J. Kelleher, C. J. Johnson, J. A. Fournier and M. A. Johnson, *J. Phys. Chem. A*, 2015, **119**, 8294-8302.
54. W. J. Zhang, G. L. Hou, P. Wang, H. G. Xu, G. Feng, X. L. Xu and W. J. Zheng, *J. Chem. Phys.*, 2015, **143**, 054302.
55. G.-L. Hou, M. Valiev and X.-B. Wang, *J. Phys. Chem. A*, 2016, **120**, 2342-2349.
56. G.-L. Hou, X.-B. Wang and M. Valiev, *J. Am. Chem. Soc.*, 2017, **139**, 11321-11324.
57. G.-L. Hou, W. Lin and X.-B. Wang, *Communications Chemistry*, 2018, **1**, 37.
58. T. I. Yacovitch, N. Heine, C. Brieger, T. Wende, C. Hock, D. M. Neumark and K. R. Asmis, *J. Chem. Phys.*, 2012, **136**, 241102.
59. W. Robertson, E. Diken, E. Price, J. Shin and M. Johnson, *Science*, 2003, **299**, 1367-1372.
60. J. W. Shin, N. I. Hammer, E. G. Diken, M. A. Johnson, R. S. Walters, T. D. Jaeger, M. A. Duncan, R. A. Christie and K. D. Jordan, *Science*, 2004, **304**, 1137-1140.
61. M. Letzner, S. Gruen, D. Habig, K. Hanke, T. Endres, P. Nieto, G. Schwaab, Ł. Walewski, M. Wollenhaupt, H. Forbert, et al., *J. Chem. Phys.*, 2013, **139**, 154304.
62. S. E. Waller, Y. Yang, E. Castracane, E. E. Racow, J. J. Kreinbihl, K. A. Nickson and C. J. Johnson, *J. Phys. Chem. Lett.*, 2018, **9**, 1216-1222.
63. Y. Yang, S. E. Waller, J. J. Kreinbihl and C. J. Johnson, *J. Phys. Chem. Lett.*, 2018, **9**, 5647-5652.
64. T. I. Yacovitch, N. Heine, C. Brieger, T. Wende, C. Hock, D. M. Neumark and K. R. Asmis, *J. Phys. Chem. A*, 2013, **117**, 7081-7090.
65. A. Kürten, A. Bergen, M. Heinritzi, M. Leiminger, V. Lorenz, F. Piel, M. Simon, R. Sitals, A. C. Wagner and J. Curtius, *Atmos. Chem. Phys.*, 2016, **16**, 12793-12813.
66. B. R. Bzdek, D. P. Ridge and M. V. Johnston, *Atmos. Chem. Phys.*, 2010, **10**, 3495-3503.
67. S. Schobesberger, A. Franchin, F. Bianchi, L. Rondo, J. Duplissy, A. Kürten, I. K. Ortega, A. Metzger, R. Schnitzhofer, J. Almeida, et al., *Atmos. Chem. Phys.*, 2015, **15**, 55-78.
68. B. M. Marsh, J. M. Voss and E. Garand, *J. Chem. Phys.*, 2015, **143**, 204201.
69. S. M. Craig, F. S. Menges and M. A. Johnson, *J. Mol. Spectrosc.*, 2017, **332**, 117-123.
70. M. J. Frisch, G. W. Trucks, H. B. Schlegel, G. E. Scuseria, M. A. Robb, J. R. Cheeseman, G. Scalmani, V. Barone, G. A. Petersson, H. Nakatsuji, et al., *Gaussian 16 Rev. B.01*, Wallingford, CT, 2016.
71. J. R. Schmidt and W. F. Polk, *WebMO Enterprise*, Holland, MI, USA, 2018.
72. C. J. Johnson and M. A. Johnson, *J. Phys. Chem. A*, 2013, **117**, 13265-13274.

73. C. J. Johnson, A. B. Wolk, J. A. Fournier, E. N. Sullivan, G. H. Weddle and M. A. Johnson, *J. Chem. Phys.*, 2014, **140**, 221101.
74. A. Masson, E. R. Williams and T. R. Rizzo, *J. Chem. Phys.*, 2015, **143**, 104313.

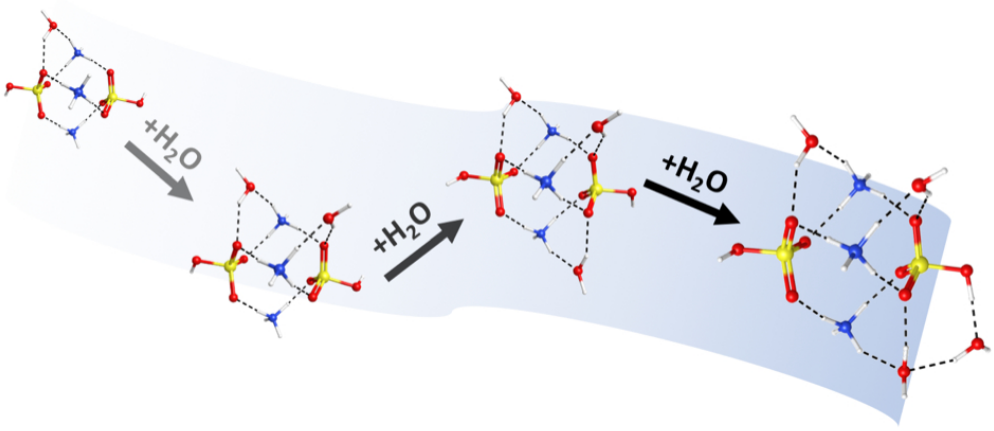

TOC Figure

80x40mm (300 x 300 DPI)